

Tracking of a Periodic RF Transmitter with a Mobile Receiver: From Theory to Implementation

François Qutin*, *Member, IEEE*, Zahra Madadi*, *Member, IEEE*, and Wee Peng Tay, *Senior Member, IEEE*

Abstract—We propose a method to track a periodic RF transmitter using a mobile receiver. By estimating the difference in time-of-arrival (TOA) of the periodic messages at different locations along its trajectory, the receiver is able to estimate the transmitter location. A major challenge lies in separating the time offset due to receiver movement from the time offset due to local oscillator (LO) drift. We propose an adaptive filtering framework that is able to track both the LO drift and the RF transmitter simultaneously, using the receiver TOA measurements and the receiver locations as inputs. Furthermore, we propose an algorithm to optimize the receiver trajectory based on the posterior Cramér-Rao lower bound. Simulation results are presented to show the feasibility of the proposed method. Finally, the proposed method is implemented on a software-defined radio (SDR) testbed. Empirical experiments demonstrate that our approach can successfully track both a static and moving transmitter to within an accuracy of less than 1 m.

Index Terms—Transmitter localization, periodic signal, local oscillator time offset, trajectory optimization, software-defined radio

I. INTRODUCTION

Localization of RF transmitters in wireless networks is an age-old problem with many potential military and civilian applications, including enemy target detection and tracking [1]–[3], spectrum sensing [4], [5], and sensor node localization [6]. Most transmitter localization techniques rely on measuring some parameter of the RF signal, and use it to infer the location of the RF transmitter. One localization method that does not require the RF transmitter to be cooperative is the use of Time-Difference-of-Arrival (TDOA) measurements. By recording the transmitted RF signal at two synchronized receivers, the difference in propagation time from the transmitter to each receiver can be measured. In this paper, we try to localize a *periodic* transmitter by designing a *virtual* TDOA (V-TDOA) system: by measuring the time-of-arrival (TOA) of the periodically transmitted message at different locations along the receiver trajectory, and compensating the TOA for the transmit period, we can determine the TDOA between those different receiver locations. By having the receiver move along an appropriate trajectory, the location of the periodic transmitter can eventually be determined. The major challenge of this otherwise simple concept is the time drift that occurs between the transmitter and the receiver due to the local

oscillator (LO) offset between transmitter and receiver. The difficulty lies in separating this LO time drift from the time offset due to V-TDOA.

The main contributions of this paper can be summarized as follows:

- We propose an algorithm to estimate the location of a periodic RF transmitter with a mobile receiver. Our algorithm relies on adaptive filtering techniques, and allows to track the location of the RF transmitter and the LO offset simultaneously. Rule-of-thumbs and simulations are presented to determine the localization accuracy.
- We investigate the optimization of the receiver trajectory to achieve the best transmitter localization accuracy. We show simulation results for different ratios of receiver-to-transmitter speed.
- The proposed localization algorithm is implemented on a software-defined radio (SDR) testbed. We show successful localization of a static transmitter, and provide experimental results for tracking of a mobile transmitter.

A. Related work

Localization of a RF transmitter usually relies on measuring some parameter of the RF signal [7]–[9]. Received signal strength (RSS) has been widely used for transmitter localization [10], [11]: RSS decreases with transmitter-to-receiver distance, and by measuring the RSS at multiple receivers it becomes possible to locate the transmitter. Unfortunately, multipath causes wide variations in RSS levels, making it difficult to relate the RSS measurement to distance. Moreover, path loss models used to relate RSS to distance need to be calibrated to the environment, and inaccurate calibration might result in poor localization performances.

Another parameter of the RF signal that can be used for localization is time-of-arrival (TOA) [7]. The TOA of an RF signal can be directly related to the distance between the transmitter and the receiver. Using TOA requires a cooperative transmitter: each receiver needs to know when the RF signal was transmitted to deduce its distance to the transmitter. TOA measurements also suffer from multipath [12], but this can be limited by using large bandwidths. In particular, ultra-wideband technology has shown promising results for RF transmitter localization using TOA [13].

Measuring the Angle-of-arrival (AOA) enables a receiver to determine the direction of the RF transmitter (if the transmitter is in line-of-sight) [9]. By using a multi-antenna array, the receiver can use the phase of the received signal at each antenna element to infer the AOA of the RF signal. The

*The first two authors made equal contributions to this paper. Preliminary versions of this work have been accepted for presentation at the IEEE International Conference on Acoustics, Speech, and Signal Processing, 2015, and the IEEE International Conference on Communications, 2015. The authors are with the School of Electrical and Electronic Engineering, Nanyang Technological University, Singapore. Emails: {fquitin, zahramadadi, wptay}@ntu.edu.sg

main advantage of AOA is that it works with non-cooperating narrowband transmitters; the main disadvantage is that it requires a MIMO array at the receiver, which comes with major form factor constraints.

Finally, time-difference-of-arrival (TDOA) consists of measuring the difference in TOA between a pair of receivers [14]–[17]. Determining TDOA is feasible when transmitters are non-cooperative, but requires the different receiver nodes to be synchronized with each other to within a few nanoseconds [18]. Such high accuracy synchronization is hard to achieve in practice. Even GPS synchronization results in TDOA errors as large as 100 ns, especially in build-up environments where having lines-of-sight to the GPS satellites may not be feasible. Recent work has investigated the use of differential TDOA (the difference in TDOA between the signals from two distinct transmitters) to use TDOA measurements in non-synchronized networks, with promising results [19].

One game-changer in RF localization is the increasing use of unmanned vehicles equipped with RF transceivers. Autonomous vehicles can determine their trajectory and movement to achieve a localization objective, thereby reducing the localization uncertainty (due to multipath or inaccurate synchronization) to arbitrarily low values [20], [21]. One example of such a localization scheme is [22], [23], where the rotation of a UAV is exploited to obtain directional RSS measurements, which are then used to localize the transmitter. Optimization of a vehicle trajectory in order to localize a transmitter has been considered for other types of measurements [24]–[26]. The information content of different measurements and the achievable localization accuracy depends significantly on the target-sensor (transmitter-receiver) trajectory. In [24], the optimal target-sensor geometries for range-only, TOA and bearing-only measurements for stationary targets are obtained based on the known position of the target. The optimization of sensor trajectory for TDOA measurements has been considered in [25], for a scenario in which two time-synchronized sensors are used for localizing a target. In [26], trajectory optimization for target tracking using a UAV and bearing-only measurements are considered. However, different types of measurements and different scenarios yield different solutions. In this paper, we consider the problem of optimal trajectory of a moving receiver for localizing a (stationary or moving) transmitter using a V-TDOA system. We take into account the effect of time offset between the receiver and transmitter LOs in the measurements in the trajectory optimization.

The concept of V-TDOA was first introduced in [27], which however considered the LO offset to be a nuisance parameter that could be ignored. As a result, the algorithms presented in [27] can only work for high-speed vehicles (such as flying UAVs) or transceiver systems with high-quality LOs. In contrast, in our work, we explicitly estimate and track the LO offset and the V-TDOA simultaneously. We build on our prior conference papers [28], [29] by including results for mobile transmitters and providing a method to optimize the receiver trajectory.

The rest of this paper is organized as follows. Section II describes the V-TDOA model and investigates the LO model used in this work. Section III presents the adaptive filter

formulation, and simulation results of our tracking method. The optimization of the receiver trajectory to achieve the best tracking accuracy is presented in Section IV. The SDR implementation and experimental results are presented in Section V. Finally, we conclude in Section VI.

II. VIRTUAL TDOA CONCEPT AND CHALLENGES

A. V-TDOA concept

We start by introducing the V-TDOA concept and defining the notations used in this paper. Consider a transmitter sending a message with periodicity T_0 . This can be a repetitive beacon sent from a transmitter in a search and rescue operation, or a synchronization signal transmitted by a base station in a cellular network. If the first message is transmitted at time t_0 , the receiver will receive the k -th message at time

$$t_k = t_0 + (k - 1)T_0 + \Delta t_k + \Delta \tau_k, \quad (1)$$

where Δt_k corresponds to the propagation time between the transmitter and the receiver, and $\Delta \tau_k$ is the time offset due to LO drift between t_0 and the time of measurement k . For a line-of-sight environment, Δt_k is defined as

$$\Delta t_k = \frac{1}{c_0} \sqrt{(x_{R,k} - x_{T,k})^2 + (y_{R,k} - y_{T,k})^2},$$

where c_0 is the speed of light, $(x_{R,k}, y_{R,k})$ are the x- and y-coordinates of the receiver, and $(x_{T,k}, y_{T,k})$ are the x- and y-coordinates of the transmitter¹. We define a *cycle* as the time period over which one message is transmitted by the transmitter (and received by the receiver). Additionally, we define the local time of the receiver LO at cycle k as

$$\tau_k \triangleq t_0 + (k - 1)T_0 + \Delta \tau_k. \quad (2)$$

From (1), we see that if the LO time offset $\Delta \tau_k$ is zero, the V-TDOA between two successive points can be estimated by evaluating $t_k - t_{k-1} - T_0$. However, due to the presence of the LO offset $\Delta \tau_k$, the challenge lies in estimating the propagation time Δt_k using the measurements t_k . Even for a static transmitter, the changes in $\Delta \tau_k$ between cycles make it impossible to solve (1) without additional information about the LO offset $\Delta \tau_k$. To overcome this problem, we use the LO model from [30] to evaluate the evolution of the LO time offset between cycles. This LO model is detailed in the next section.

B. LO offset model

We begin by describing the LO model used in this paper. We simplify the three-state LO model from [30] to a two-state model, which is sufficient to capture the LO dynamics of our system [31], [32]. The stochastic differential equations describing the two-state LO model are written as

$$\begin{cases} d\tau(t) &= \beta(t)dt + q_1 dw_1(t) \\ d\beta(t) &= q_2 dw_2(t) \end{cases} \quad (3)$$

¹In this paper, we discuss only tracking in a two dimensional space. Our formulation can however be easily extended to tracking in a three dimensional space.

where $\tau(t)$ and $\beta(t)$ are the LO local time and LO skew at time t , and q_1 and q_2 are the process noise parameters that correspond to white frequency noise and random walk frequency noise, respectively. The noise terms $w_1(t)$, $w_2(t)$ are two independent, one-dimensional standard Wiener processes, each one defined as a Gaussian process with stationary independent increments such that $w(t) - w(s) \sim \mathcal{N}(0, t - s)$ and $w(0) = 0$.² Additionally, the integration of a Wiener process $\int_a^b w(t)dt$ is distributed as $\mathcal{N}(0, (b - a)^3/3)$. The system in (3) is a strictly linear stochastic differential equation. Hence, its solution is given by [30]

$$\begin{cases} \tau(t + T_0) = \tau(t) + T_0\beta(t) + q_1 n_\tau(t, T_0), \\ \beta(t + T_0) = \beta(t) + q_2 n_\beta(t, T_0). \end{cases} \quad (4)$$

Given the above-mentioned properties of Wiener processes, the noise vector $\mathbf{n}(t, T_0) = [n_\tau(t, T_0) \ n_\beta(t, T_0)]^T$ can then be shown to be distributed as $\mathbf{n}(t, T_0) \sim \mathcal{N}(0, \mathbf{Q}_{\text{LO}})$ (see equations (8)-(9) in [30]) with \mathbf{Q}_{LO} equal to

$$\mathbf{Q}_{\text{LO}} = q_1^2 \begin{bmatrix} T_0 & 0 \\ 0 & 0 \end{bmatrix} + q_2^2 \begin{bmatrix} \frac{T_0^3}{3} & \frac{T_0^2}{2} \\ \frac{T_0^2}{2} & T_0 \end{bmatrix} \quad (5)$$

From (4) we see that, for low noise terms, the LO local time τ drifts quasi-linearly. By combining this information with the measurements (1), it becomes possible to use an adaptive filtering framework that will estimate the term Δt_k while tracking the LO offset term $\Delta\tau_k$.

III. PERIODIC TRANSMITTER TRACKING METHOD

In this section, we introduce a system model that allows a receiver to track the transmitter location $(x_{T,k}, y_{T,k})$ while tracking the LO offset $\Delta\tau_k$. Using the LO model introduced in Section II-B, a state-space model and measurement model are proposed and integrated in an adaptive filtering framework.

A. Process and measurement model

Process model: For the general case of a moving transmitter, the state to be estimated at cycle k is defined as

$$\mathbf{x}_k = [\tau_k, \beta_k, x_{T,k}, \dot{x}_{T,k}, y_{T,k}, \dot{y}_{T,k}]^T, \quad (6)$$

where $x_{T,k}$ and $y_{T,k}$ are the x- and y-coordinates of the transmitter, respectively, and $\dot{x}_{T,k}$ and $\dot{y}_{T,k}$ are the x- and y-coordinate speed of the transmitter, respectively. We consider a constant-velocity model, such that the process model can be described as

$$\mathbf{x}_k = \mathbf{F}\mathbf{x}_{k-1} + \mathbf{w}_k(\mathbf{Q}), \quad (7)$$

where

$$\mathbf{F} = \mathbf{I}_3 \otimes \begin{bmatrix} 1 & T_0 \\ 0 & 1 \end{bmatrix}$$

with \mathbf{I}_3 being a 3×3 identity matrix and \otimes denoting the Kronecker product. The covariance matrix of the process noise \mathbf{Q} can be defined as

$$\mathbf{Q} = \begin{bmatrix} \mathbf{Q}_{\text{LO}} & \mathbf{0}_{4 \times 4} \\ \mathbf{0}_{2 \times 2} & \mathbf{Q}_{\text{Tx}} \end{bmatrix} \quad (8)$$

²We use $\mathcal{N}(\mu, \sigma^2)$ to denote a Gaussian distribution with mean μ and variance σ^2 .

in which \mathbf{Q}_{LO} is the 2×2 matrix defined in (5) and \mathbf{Q}_{Tx} is the covariance matrix related to transmitter motion defined as

$$\mathbf{Q}_{\text{Tx}} = \begin{bmatrix} \sigma_{a,x}^2 & 0 \\ 0 & \sigma_{a,y}^2 \end{bmatrix} \otimes \begin{bmatrix} \frac{T_0^4}{4} & \frac{T_0^3}{2} \\ \frac{T_0^3}{2} & T_0^2 \end{bmatrix},$$

where $\sigma_{a,x}^2$ and $\sigma_{a,y}^2$ are the variances of random acceleration in the x and y directions, respectively.

Measurement model: At each cycle of the algorithm, the receiver measures the TOA of the transmitted message. The noiseless TOA t_k is given by

$$\begin{aligned} t_k &= h_k(\mathbf{x}_k) \\ &\triangleq \tau_k + \frac{1}{c_0} \sqrt{(x_{R,k} - x_{T,k})^2 + (y_{R,k} - y_{T,k})^2}. \end{aligned} \quad (9)$$

The measured TOA at the receiver \hat{t}_k can then be expressed as

$$\hat{t}_k = h_k(\mathbf{x}_k) + v_k(R) \quad (10)$$

where $v_k(R)$ is the zero-mean Gaussian measurement noise with variance R . In (10), $h_k(\mathbf{x}_k)$ is a nonlinear function of \mathbf{x}_k , which will have important consequences for the adaptive filter design.

B. Kalman filter, EKF and UKF

The problem at hand is determining the state \mathbf{x}_k based on the measurements \hat{t}_k (all the measurements up to cycle k). In a Bayesian framework, the tracking problem is to recursively estimate \mathbf{x}_k based on all the measurements $\hat{t}_{(1:k)}$, up to cycle k . This can be achieved by maximizing the conditional density $p(\mathbf{x}_k | \hat{t}_{(1:k)})$ of the state \mathbf{x}_k . It is well-known that if the process model and measurement model are linear, and that the process noise and measurement noise are Gaussian random variables, the Kalman filter provides the optimal solution to this problem. The Kalman filter decomposes the problem into a two-stage process, consisting of a prediction stage

$$p(\mathbf{x}_k | \hat{t}_{(1:k-1)}) = \int p(\mathbf{x}_k | \mathbf{x}_{k-1}) p(\mathbf{x}_{k-1} | \hat{t}_{(1:k-1)}) d\mathbf{x}_{k-1}, \quad (11)$$

and an update stage

$$p(\mathbf{x}_k | \hat{t}_{(1:k)}) \propto p(\hat{t}_k | \mathbf{x}_k) p(\mathbf{x}_k | \hat{t}_{(1:k-1)}), \quad (12)$$

which results in a set of fairly simple recursive equations involving the process and measurement model matrices. In our problem, however, the measurement model (10) is nonlinear, which requires the use of nonlinear Kalman filtering techniques. In this paper, we will consider two types of adaptive filters: the extended Kalman filter (EKF) and the unscented Kalman filter (UKF) [33].

The principle of an EKF is to linearize the nonlinear model (in this case the measurement model) around the current state. The prediction stage (11) can then be expressed as

$$\mathbf{x}_{k|k-1} = \mathbf{F}\mathbf{x}_{k-1|k-1} \quad (13a)$$

$$\mathbf{P}_{k|k-1} = \mathbf{F}\mathbf{P}_{k-1|k-1}\mathbf{F}^T + \mathbf{Q} \quad (13b)$$

where $\mathbf{P}_{k|k}$ represents the state error covariance matrix (or the uncertainty on the state $\mathbf{x}_{k|k}$). The update stage (12) can then be written as

$$\mathbf{K}_k = \mathbf{P}_{k|k-1} \mathbf{H}_k^T (\mathbf{H}_k \mathbf{P}_{k|k-1} \mathbf{H}_k^T + R)^{-1} \quad (14a)$$

$$\mathbf{x}_{k|k} = \mathbf{x}_{k|k-1} + \mathbf{K}_k (\hat{t}_k - \mathbf{H}_k \mathbf{x}_{k|k-1}) \quad (14b)$$

$$\mathbf{P}_{k|k} = (\mathbf{I} - \mathbf{K}_k \mathbf{H}_k) \mathbf{P}_{k|k-1} \quad (14c)$$

where

$$\mathbf{H}_k = \left. \frac{\partial h_k(\mathbf{x})}{\partial \mathbf{x}} \right|_{\mathbf{x}=\mathbf{x}_{k|k-1}} \quad (15)$$

is the Jacobian matrix of $h_k(\mathbf{x})$ evaluated at $\mathbf{x} = \mathbf{x}_{k|k-1}$. Although very simple, the process of propagating the state covariance matrix $\mathbf{P}_{k|k}$ through the ‘‘linearized model’’ often introduces a significant error in the state covariance, resulting in eventual divergence of the filter. We will see in the experimental results that, although the EKF works fine for localizing a static transmitter, the UKF provides better performances for a moving transmitter.

The UKF is an extension of the EKF that does not suffer as much from propagation of the covariance error matrix through a ‘‘linearized model’’. The principle is the following: the state estimate is augmented with a set of sigma-points, whose location around the mean state are chosen to match the state covariance, and both the state and the sigma-points are propagated through the process and measurement model (which may be nonlinear). The covariance is then computed based on the sigma-points. We first define the augmented state and augmented covariance matrix:

$$\mathbf{x}_{k-1|k-1}^A = [\mathbf{x}_{k-1|k-1} \quad \mathbb{E}\{v_k\}]^T \quad (16a)$$

$$\mathbf{P}_{k-1|k-1}^A = \begin{bmatrix} \mathbf{P}_{k-1|k-1} & \mathbf{0}_{6 \times 1} \\ \mathbf{0}_{1 \times 6} & R \end{bmatrix} \quad (16b)$$

where the last term of the augmented state is the mean of the additive measurement noise, which in this case is $\mathbb{E}\{v_k\} = 0$. The sigma-points are derived as follows:

$$\begin{cases} \chi_{k-1|k-1}^{A,0} = \mathbf{x}_{k-1|k-1}^A, \\ \chi_{k-1|k-1}^{A,i} = \mathbf{x}_{k-1|k-1}^A + \sqrt{(L+\lambda)\mathbf{P}_{k-1|k-1}^A}, \\ \quad \text{for } i = 1, \dots, L, \\ \chi_{k-1|k-1}^{A,i} = \mathbf{x}_{k-1|k-1}^A - \sqrt{(L+\lambda)\mathbf{P}_{k-1|k-1}^A}, \\ \quad \text{for } i = L+1, \dots, 2L, \end{cases} \quad (17)$$

where L is the dimension of the state plus the dimension of the noise, and $\lambda = \alpha^2(L + \kappa) - L$ with $\alpha = 10^{-3}$ and $\kappa = 0$ controlling the spread of the sigma-points. The matrix square root in (17) is the lower triangular matrix of the Cholesky decomposition of the matrix. The augmented-state sigma-points are decomposed into sigma-points state components $\chi_{k-1|k-1}^i$ and sigma-points noise components $\chi_{k-1|k-1}^{n,i}$:

$$\chi_{k-1|k-1}^{A,i} = [(\chi_{k-1|k-1}^i)^T \quad (\chi_{k-1|k-1}^{n,i})^T]^T \quad (18)$$

The prediction stage for each sigma-point $i = 0, \dots, 2L$ is defined as

$$\chi_{k|k-1}^i = \mathbf{F} \chi_{k-1|k-1}^i \quad i = 0, \dots, 2L \quad (19)$$

and the predicted state and state covariance can be obtained as

$$\mathbf{x}_{k|k-1} = \sum_{i=0}^{2L} W_s^i \chi_{k|k-1}^i \quad (20a)$$

$$\mathbf{P}_{k|k-1} = \sum_{i=0}^{2L} W_c^i (\chi_{k|k-1}^i - \mathbf{x}_{k|k-1})(\chi_{k|k-1}^i - \mathbf{x}_{k|k-1})^T \quad (20b)$$

where $W_s^i = W_c^i = \frac{1}{2(L+\lambda)}$, $W_s^0 = \frac{\lambda}{L+\lambda}$ and $W_c^0 = \frac{\lambda}{L+\lambda} + (1 - \alpha^2 + \beta)$ with $\beta = 2$. During the update stage, the sigma-points are projected through the observation function $h_k(\mathbf{x}_k)$, and the additive measurement noise for each sigma-point is added:

$$\gamma_k^i = h_k(\chi_{k|k-1}^i) + \chi_{k-1|k-1}^{n,i} \quad i = 0, \dots, 2L \quad (21)$$

The weighted observations of the sigma-points are then combined to determine the UKF Kalman gain:

$$z_k = \sum_{i=0}^{2L} W_s^i \gamma_k^i, \quad (22a)$$

$$\mathbf{P}_{z_k z_k} = \sum_{i=0}^{2L} W_c^i (\gamma_k^i - z_k)(\gamma_k^i - z_k)^T, \quad (22b)$$

$$\mathbf{P}_{\mathbf{x}_k z_k} = \sum_{i=0}^{2L} W_c^i (\chi_{k|k-1}^i - \mathbf{x}_{k|k-1})(\gamma_k^i - z_k)^T, \quad (22c)$$

$$\mathbf{K}_k = \mathbf{P}_{\mathbf{x}_k z_k} \mathbf{P}_{z_k z_k}^{-1}. \quad (22d)$$

The updated state and state covariance are then evaluated as

$$\mathbf{x}_{k|k} = \mathbf{x}_{k|k-1} + \mathbf{K}_k (\hat{t}_k - z_k), \quad (23a)$$

$$\mathbf{P}_{k|k} = \mathbf{P}_{k|k-1} - \mathbf{K}_k \mathbf{P}_{z_k z_k} \mathbf{K}_k^T \quad (23b)$$

Since in the UKF, the sigma-points are propagated through the nonlinear function $h_k(\mathbf{x}_k)$, the recovered state and state covariance are a better representation of the real underlying state and state covariance. We will see in the experimental results that the UKF is more robust when tracking a moving transmitter.

C. Steady-state LO tracking error prediction

One of the main advantages of the linear Kalman filter is its predictability: if the filter is observable and controllable, the Kalman filter is guaranteed to converge. Moreover, the state covariance error matrix is guaranteed to converge to the solution of the discrete algebraic Riccati equation (DARE), which is independent of the state and can be computed *a priori* based only on the process model and measurement model. Unfortunately, no such guarantees can be given for nonlinear EKFs or UKFs. In order to provide some insight into the working and steady-state prediction error of our nonlinear filters, we consider the simplified two-state system, composed only of the local LO time and LO skew $\mathbf{x}_{\text{LO},k} = [\tau_k \quad \beta_k]^T$. Based on (4), the process model is described by

$$\mathbf{x}_{\text{LO},k+1} = \mathbf{F}_{\text{LO},k} \mathbf{x}_{\text{LO},k} + \mathbf{n}_k(\mathbf{Q}_{\text{LO}}) \quad (24)$$

with $\mathbf{F}_{\text{LO},k} = [1 \ T_0, 0 \ 1]$. If we do not consider the effect of transmitter and receiver movement in our system, the TOA measurement of our two-state system can be expressed as

$$\hat{t}_{\text{LO},k} = \mathbf{H}_{\text{LO}}\mathbf{x}_{\text{LO},k} + v_k(R) \quad (25)$$

where $\mathbf{H}_{\text{LO}} = [1 \ 0]$. It can easily be verified that the Kalman filter defined by (24)-(25) is fully observable and controllable [34]. In that case, the state error covariance matrix $\mathbf{P}_{\text{LO},k|k}$ of the simplified Kalman filter is guaranteed to converge towards the steady-state error covariance matrix, which can be obtained by solving the DARE given by:

$$\mathbf{P}_{\text{LO},k+1|k+1} = \mathbf{F}_{\text{LO}}\mathbf{P}_{\text{LO},k|k}\mathbf{F}_{\text{LO}}^T - \mathbf{F}_{\text{LO}}\mathbf{P}_{\text{LO},k|k}\mathbf{H}_{\text{LO}}^T (\mathbf{H}_{\text{LO}}\mathbf{P}_{\text{LO},k|k}\mathbf{H}_{\text{LO}}^T + R)^{-1} \mathbf{H}_{\text{LO}}\mathbf{P}_{\text{LO},k|k}\mathbf{F}_{\text{LO}}^T + \mathbf{Q}_{\text{LO}} \quad (26)$$

In the following experiment, we measure the LO drift with the setup described in Section V. The transmitter and the receiver are connected with a cable, so that the only drift is due to the LO offset (and not to transmitter-receiver movement). The LO time and skew are tracked with the Kalman filter described by the process and measurement model (24)-(25). Figure 1 shows the elements of the state covariance matrix $\mathbf{P}_{\text{LO},k|k}$, as well as the solution of the DARE obtained by using Matlab's DARE solver. It can be seen that the elements of $\mathbf{P}_{\text{LO},k|k}$ quickly converges to the solution of the DARE. We

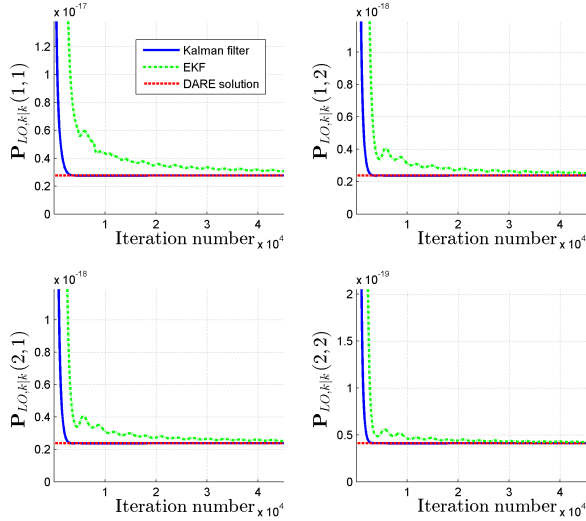


Fig. 1. Elements of the state covariance matrix related to the LO states for the Kalman filter, EKF and DARE solution.

then simulate the full system by adding the time offset due to transmitter-receiver movement to the measured LO drift, as detailed in the simulation results in Section III-D. The first 2×2 submatrix of $\mathbf{P}_{k|k}$ is plotted on Figure 1. It can be seen that, when the EKF converges, the state error corresponding to the LO states (τ_k and β_k) converges to the solution predicted by the DARE. Given the measurement model (9)-(10), in the worst case, all the error on τ_k will propagate on the transmitter-to-receiver distance r

$$r = \sqrt{(x_{R,k} - x_{T,k})^2 + (y_{R,k} - y_{T,k})^2} \quad (27)$$

with a factor c_0 , which will determine the transmitter localization error. This leads to the following rule-of-thumb.

Rule-of-thumb: when the EKF converges, the error on the transmitter location estimate has a worst-case variance equal to

$$\sigma_r^2 = c_0^2 \cdot \mathbf{P}_{\text{LO},k|k}(1,1) \quad (28)$$

where $\mathbf{P}_{\text{LO},k|k}(1,1)$ can be obtained by solving the DARE of the “equivalent” linear Kalman filter defined by (24)-(25).

D. Simulations and discussion

We first evaluate the performances of the proposed localization method through simulations. It should be noted that, for all simulations, the transmitter and receiver movement are simulated, but that the LO drift used in the simulations is a real LO drift measured with our setup described in Section V. The transmitter and receiver were connected with a cable, and the TOAs of the periodic messages were estimated. Since the cable length is fixed, the measured TOA values contain only the effects of LO drift (and no effect of transmitter or receiver movement). These measured TOA values are used to model the LO drift in our simulations.

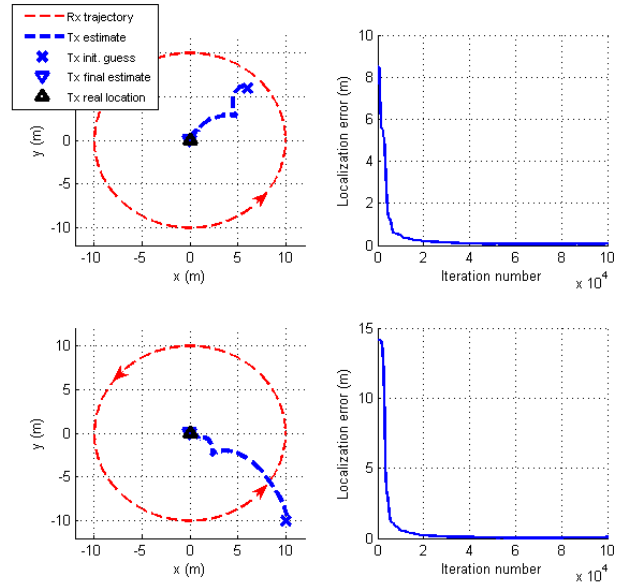


Fig. 2. Position estimation of a static transmitter placed at $(0, 0)$, from two different initial guess $(x_0, y_0) = (6, 6)$ and $(10, -10)$.

In the first simulation, we assume a static transmitter at location $(0, 0)$ transmitting a periodic signal with period $T_0 = 10$ ms. The receiver moves around the transmitter with a speed of 1.5 m/s. The receiver trajectory is a circle with its origin at $(0, 0)$ and radius 10 m. The measurement noise variance of our setup (described in Section V) is found to be $(5 \text{ ns})^2$ in a multipath-free environment, but TOA estimation in real environments will always suffer from multipath. To account for this, the measurement noise variance in our simulations (as well as in our EKF/UKF design) is set equal to $R = (40 \text{ ns})^2$. The results obtained when using the EKF are shown in

Figure 2. The red solid curve represents the receiver trajectory, the blue dashed curve represents the estimated transmitter location and the black square represents the real transmitter location. The results in this figure are related to two different initial guesses $(x_0, y_0) = (7, 7)$ and $(x_0, y_0) = (15, 15)$ for the transmitter location, and are marked by crosses in the figure. The estimation errors (difference between real value and the estimated one) in r are also plotted as a function of the cycle number. It can be seen that the EKF is able to successfully localize the transmitter in both simulations.

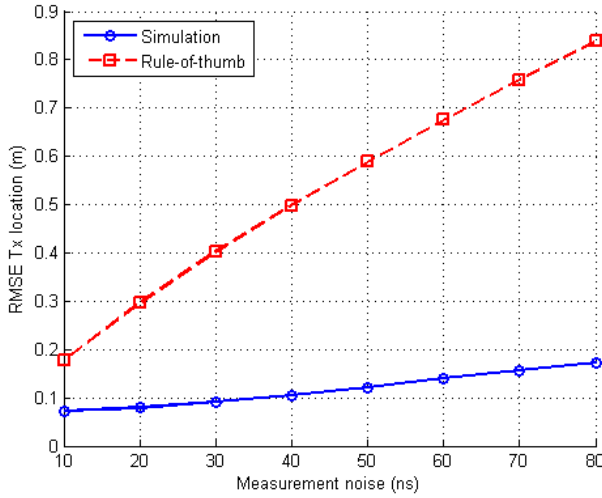


Fig. 3. Tx localization RMSE vs measurement noise standard deviation.

The result of the DARE for the “equivalent” linear Kalman filter is given in Figure 1. We can see that $\mathbf{P}_{LO,k|k}(1, 1) = (1.66 \text{ ns})^2$. According to our rule-of-thumb, the corresponding transmitter localization estimate has an error with variance of $\sigma_r^2 = (0.50 \text{ m})^2$. We evaluate the effectiveness of our rule-of-thumb by running a large number of realizations of the simulation in Figure 2 (with random initial guesses), and by measuring the error of the steady-state localization error (after convergence). The RMSE of the steady-state localization is equal to $(0.11 \text{ m})^2$. This is well within the bounds of the solution provided by our rule-of-thumb. Figure 3 shows the transmitter localization RMSE versus the measurement noise standard deviation \sqrt{R} . The bound predicted by our rule-of-thumb is provided for comparison. It can be seen that the RMSE is well below the bound of our rule-of-thumb in all cases.

In the following simulation, we consider a moving transmitter sending a periodic message with period $T_0 = 10$ ms. The transmitter starts at location $(0, 0)$ and we consider two values for the transmitter’s speed: $v_T = 0.025$ m/s and 0.5 m/s. The transmitter moves in a straight line (according to the process model) in one scenario, and along an arc (deviating from the process model) in another. The receiver moves in a circular trajectory centered at $(0, 0)$ and radius 10 m at a speed of 1.5 m/s. We suppose that the receiver knows the initial location of the transmitter, but has no information about the transmitter’s motion. The simulation results when using the EKF are shown in Figure 4. It can be seen that the receiver is able to estimate and track the transmitter’s motion when

the transmitter speed is low. For higher transmitter speed, the accuracy of the estimation is decreased. This is mostly due to the fact that the movement of the receiver is small compared to the movement of the transmitter, resulting in a poor geometry for localizing the transmitter. Note that in the case of a moving transmitter, the EKF parameters $\sigma_{a,x}$ and $\sigma_{a,y}$ have to be increased such that the process model is able to match the transmitter movement.

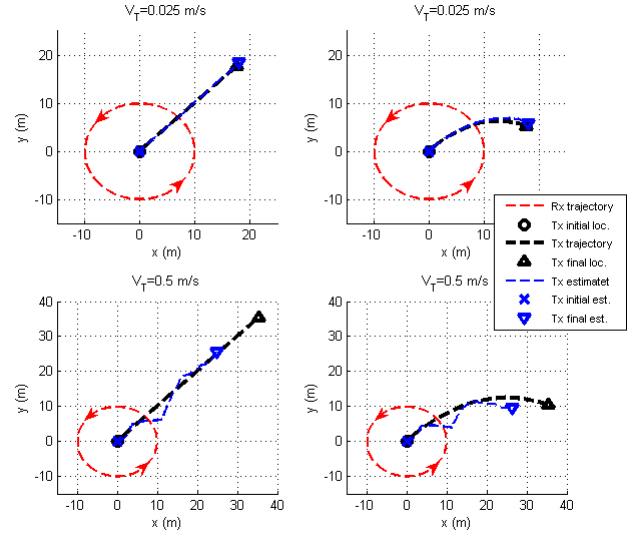


Fig. 4. Position estimation of a moving transmitter starting at $(0, 0)$ with different speeds $v_T = 0.025$ and 0.5 m/s.

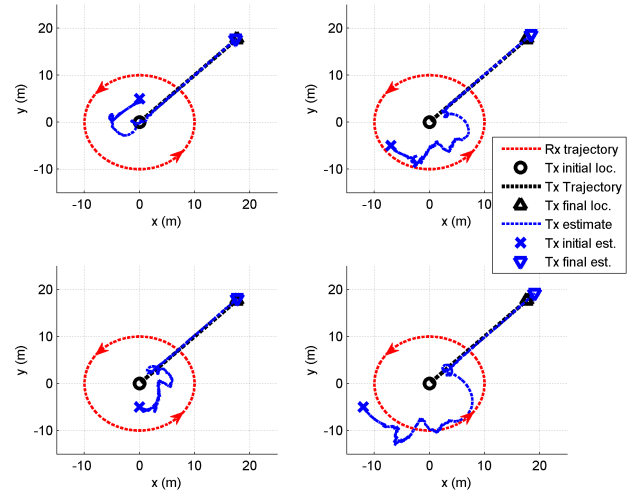


Fig. 5. Position estimation of a moving transmitter with speed $v_T = 0.025$ m/s with different initial guesses.

In another simulation, we consider a moving transmitter with speed $v_T = 0.025$ m/s sending a periodic message with period $T_0 = 10$ ms. The transmitter starts at location $(0, 0)$ but in our simulation, the initial estimate of the transmitter’s location is assumed not to be the correct value. We consider different initial estimates as observed in Figure 5. It can

be seen that the receiver is able to estimate and track the transmitter's motion even when the initial estimate of the transmitter's location is incorrect.

IV. RECEIVER TRAJECTORY OPTIMIZATION

Estimating the position of a transmitter from noisy measurements with the method described in Section III highly depends on the transmitter-receiver geometry. In this section, we consider the problem of receiver trajectory optimization in order to achieve the best transmitter tracking performance. Posterior Cramér-Rao lower bound (PCRLB) defines a limit on the performance of any Bayesian estimator for a given dynamic system with discrete-time dynamics and measurement model as follows:

$$\begin{aligned}\mathbf{x}_k &= f_k(\mathbf{x}_k, \mathbf{w}_k) \\ \mathbf{z}_k &= h_k(\mathbf{x}_k, \mathbf{v}_k)\end{aligned}$$

where f_k and h_k are the process and measurement models respectively, with measurement vector \mathbf{z}_k , process noise \mathbf{w}_k , and measurement noise \mathbf{v}_k at time step k .

Conventional (unconditional) PCRLB [35] that averages out the measurement information is an off-line bound that depends only on the system process model, measurement model and prior knowledge of the system state at the initial time step. The mean square error (MSE) of any Bayesian estimator satisfies

$$\mathbb{E}\{[\hat{\mathbf{x}}(\mathbf{z}) - \mathbf{x}][\hat{\mathbf{x}}(\mathbf{z}) - \mathbf{x}]^T\} \geq \mathbf{J}^{-1} \quad (29)$$

where $\hat{\mathbf{x}}$ is the estimator of \mathbf{x} , $\mathbf{J} = \mathbb{E}\{-\Delta_{\mathbf{x}}^{\mathbf{x}} \log p(\mathbf{x}, \mathbf{z})\}$ is the Fisher information matrix (FIM), and we use the operator $\Delta_{\mathbf{x}}^{\mathbf{y}}$ to denote $\nabla_{\mathbf{x}} \nabla_{\mathbf{y}}^T$. Note that the expectation in (29) is with respect to the joint distribution $p(\mathbf{x}, \mathbf{z})$.

On the other hand, the conditional PCRLB [36] utilizes the information in the measurements up to the current time step to determine a bound on the MSE of any Bayesian estimator at the next time step. The conditional PCRLB for estimating a random state vector \mathbf{x}_k and measurement vector \mathbf{z}_k is defined as

$$\mathbb{E}\{(\hat{\mathbf{x}}_k - \mathbf{x}_k)(\hat{\mathbf{x}}_k - \mathbf{x}_k)^T \mid \mathbf{z}_{1:k-1}\} \geq \mathbf{L}^{-1}(\mathbf{x}_k \mid \mathbf{z}_{1:k-1}),$$

where $\hat{\mathbf{x}}_k$ is the estimator of state \mathbf{x}_k given the measurements $\mathbf{z}_{1:k-1}$ up to time $k-1$. Following [36], let

$$\mathbf{I}(\mathbf{x}_{0:k} \mid \mathbf{z}_{1:k-1}) \triangleq \mathbb{E}\{-\Delta_{\mathbf{x}_{0:k}}^{\mathbf{x}_{0:k}} \log p(\mathbf{x}_{0:k}, \mathbf{z}_k \mid \mathbf{z}_{1:k-1})\},$$

where $\mathbf{x}_{0:k}$ denotes the state vectors up to time k . Let L_x be the length of state vector \mathbf{x}_k . Then, the conditional PCRLB $\mathbf{L}^{-1}(\mathbf{x}_k \mid \mathbf{z}_{1:k-1})$ is equal to the $L_x \times L_x$ lower right-block of $\mathbf{I}^{-1}(\mathbf{x}_{0:k} \mid \mathbf{z}_{1:k-1})$.

Computation of the conditional PCRLB $\mathbf{L}^{-1}(\mathbf{x}_k \mid \mathbf{z}_{1:k-1})$ directly requires computing the inverse of matrix \mathbf{I} with dimension $L_x(k+1) \times L_x(k+1)$, which is computationally expensive. The interested reader can refer to [36] for more details. In [37], a recursive form, which is computationally much simpler, was derived as an approximation for the conditional PCRLB:

$$\begin{aligned}\mathbf{L}^{-1}(\mathbf{x}_k \mid \mathbf{z}_{1:k-1}) &\approx \mathbf{B}_{k-1}^{22} \\ &- \mathbf{B}_{k-1}^{21} [\mathbf{B}_{k-1}^{11} + \mathbf{L}(\mathbf{x}_{k-1} \mid \mathbf{z}_{1:k-2})]^{-1} \mathbf{B}_{k-1}^{12} \quad (30)\end{aligned}$$

where

$$\begin{aligned}\mathbf{B}_{k-1}^{11} &= \mathbb{E}\{-\Delta_{\mathbf{x}_{k-1}}^{\mathbf{x}_{k-1}} \log p(\mathbf{x}_k \mid \mathbf{x}_{k-1})\} \\ \mathbf{B}_{k-1}^{12} &= \mathbb{E}\{-\Delta_{\mathbf{x}_{k-1}}^{\mathbf{x}_k} \log p(\mathbf{x}_k \mid \mathbf{x}_{k-1})\} = (\mathbf{B}_{k-1}^{21})^T \\ \mathbf{B}_{k-1}^{22} &= \mathbb{E}\{-\Delta_{\mathbf{x}_k}^{\mathbf{x}_k} [\log p(\mathbf{x}_k \mid \mathbf{x}_{k-1}) + \log p(\mathbf{z}_k \mid \mathbf{x}_k)]\},\end{aligned}$$

and the above expectations are taken over $p(\mathbf{x}_{0:k}, \mathbf{z}_k \mid \mathbf{z}_{1:k-1})$.

In our problem as presented in Section III, the state transition model is linear, the process noise is additive Gaussian, and the measurement model is nonlinear. Under these assumptions, it can be shown that the conditional Fisher information in (30) can be approximated as

$$\begin{aligned}\mathbf{L}(\mathbf{x}_k \mid \hat{t}_{1:k-1}) &\approx (\mathbf{Q} + \mathbf{F}(\mathbf{L}(\mathbf{x}_{k-1} \mid \hat{t}_{1:k-2}))^{-1} \mathbf{F}^T)^{-1} \\ &+ \mathbb{E}\{-\Delta_{\mathbf{x}_k}^{\mathbf{x}_k} \log p(\hat{t}_k \mid \mathbf{x}_k)\}, \quad (31)\end{aligned}$$

where \mathbf{F} is the state transition matrix and \mathbf{Q} is the covariance matrix of the process noise as defined in Section III.

To compute the last term in the conditional FIM given in (31), from (10), we know that the measurement noise is zero-mean Gaussian with covariance R , therefore we have

$$p(\hat{t}_k \mid \mathbf{x}_k) = \frac{1}{\sqrt{2\pi R}} \times \exp\left\{-\frac{(\hat{t}_k - h_k(\mathbf{x}_k))^2}{2R}\right\} \quad (32)$$

and it can be shown that

$$\begin{aligned}-\Delta_{\mathbf{x}_k}^{\mathbf{x}_k} \log p(\hat{t}_k \mid \mathbf{x}_k) &= -\frac{1}{R} (\Delta_{\mathbf{x}_k}^{\mathbf{x}_k} h_k(\mathbf{x}_k))^T (\hat{t}_k - h_k(\mathbf{x}_k)) + \\ &\frac{1}{R} (\nabla_{\mathbf{x}_k} h_k(\mathbf{x}_k))^T \nabla_{\mathbf{x}_k} h_k(\mathbf{x}_k) \quad (33)\end{aligned}$$

By replacing (33) in (31), the recursive form of the approximate conditional FIM can be written as

$$\mathbf{L}_k = (\mathbf{Q} + \mathbf{F} \mathbf{L}_{k-1}^{-1} \mathbf{F}^T)^{-1} + \frac{1}{R} (\nabla_{\mathbf{x}_k} h_k(\mathbf{x}_k))^T \nabla_{\mathbf{x}_k} h_k(\mathbf{x}_k). \quad (34)$$

The conditional FIM equation in (34) implies that information at each time step consists of two parts: the first term that relates to the prediction part (prior information) and the second term that comes from current measurement (update).

In (34), the initial (conditional) FIM \mathbf{L}_0 is computed as

$$\mathbf{L}_0 = E\{[\nabla_{\mathbf{x}_0} \log p(\mathbf{x}_0)][\nabla_{\mathbf{x}_0} \log p(\mathbf{x}_0)]^T\}$$

where expectation is respect to $p(\mathbf{x}_0)$. For the initial Gaussian distribution $p(\mathbf{x}_0)$ with mean $\bar{\mathbf{x}}$ and covariance $\mathbf{P}_{0|0}$, $\mathcal{N}(\bar{\mathbf{x}}, \mathbf{P}_{0|0})$, it follows that

$$\begin{aligned}\mathbf{L}_0 &= E\{\mathbf{P}_{0|0}^{-1}(\mathbf{x}_0 - \bar{\mathbf{x}}_0)[\mathbf{P}_{0|0}^{-1}(\mathbf{x}_0 - \bar{\mathbf{x}}_0)]^T\} \\ &= \mathbf{P}_{0|0}^{-1} E\{(\mathbf{x}_0 - \bar{\mathbf{x}}_0)(\mathbf{x}_0 - \bar{\mathbf{x}}_0)^T\} \mathbf{P}_{0|0}^{-1} \\ &= \mathbf{P}_{0|0}^{-1} \mathbf{P}_{0|0} \mathbf{P}_{0|0}^{-1} = \mathbf{P}_{0|0}^{-1}.\end{aligned} \quad (35)$$

A. Optimizing receiver trajectory

The receiver trajectory must be chosen carefully to improve localization performance and convergence of the EKF/UKF. The objective of this subsection is to determine which trajectories maximize the amount of information provided by the measurements and result in optimal target localization and tracking. We consider the trace of the approximate conditional PCRLB (given by the inverse of \mathbf{L}_k in (34)) as the objective

function. The eigenvectors of the conditional PCRLB are the axes of the uncertainty ellipsoid of the parameters to be estimated, and their corresponding eigenvalues are the lengths of the axes. The trace of the conditional PCRLB represents the average variance of the estimates [24]. The computation of \mathbf{L}_k in (34) is based on the true positions of the transmitter. However, in this problem the true positions of the transmitter is unknown and our goal is to estimate them. Therefore, at each time step k , we use the predicted state $\mathbf{x}_{k|k-1}$ of the transmitter in the computation of \mathbf{L}_k to obtain

$$\begin{aligned} \hat{\mathbf{L}}_k &= \left(\mathbf{Q} + \mathbf{F}\hat{\mathbf{L}}_{k-1}^{-1}\mathbf{F}^T \right)^{-1} + \frac{1}{R} \left(\nabla_{\mathbf{x}_k} h_k(\mathbf{x}_{k|k-1}) \right)^T \\ \nabla_{\mathbf{x}_k} h_k(\mathbf{x}_{k|k-1}) &= \left(\mathbf{Q} + \mathbf{F}\hat{\mathbf{L}}_{k-1}^{-1}\mathbf{F}^T \right)^{-1} + \frac{1}{R} \mathbf{H}_k^T \mathbf{H}_k. \end{aligned} \quad (36)$$

Depending on the application, different constraints can be added to the receiver trajectory optimization problem. In this paper, as a proof of concept, we consider the following minimization problem for optimizing the receiver trajectory:

$$\min_{x_{R,k}, y_{R,k}} \text{trace}(\hat{\mathbf{L}}_k^{-1}) \quad (37a)$$

subject to

$$(x_{R,k} - x_{T,k})^2 + (y_{R,k} - y_{T,k})^2 \geq d_{\min}^2, \quad (37b)$$

$$(x_{R,k} - x_{R,k-1})^2 + (y_{R,k} - y_{R,k-1})^2 \leq v_{R,\max}^2 T_0^2, \quad (37c)$$

where $x_{T,k}$ and $y_{T,k}$ are the third and fifth components in the predicted state $\mathbf{x}_{k|k-1}$ (i.e., the predicted x- and y-coordinates of the transmitter, respectively), d_{\min} is the minimum distance between the receiver and transmitter, and $v_{R,\max}$ is the maximum speed of the receiver. This corresponds to many practical applications, including stealth tracking, in which the receiver is required to maintain a minimum distance from the transmitter. In our simulations and experiments, we consider only scenarios in which the constraints (37b)-(37c) are feasible.

Using the estimated position of the transmitter at each time step, the estimated value of the conditional FIM defined above is used in the objective function (37a) to find the optimum position of the receiver at the next time step. Given the non-linearity of the objective function and the constraints, different numerical methods (such as gradient descent) can be used to solve the optimization problem.

B. Simulations and discussion

In this section, we consider different scenarios for localization and tracking of both a static and a moving transmitter. At the same time, we determine the optimum trajectory of the receiver in each scenario for tracking of the transmitter. In all the scenarios considered in this section, the minimum distance and measurement noise are set as $d_{\min} = 8$ m and $\sigma_n = 40$ ns. We use the EKF developed in Section III-B as the transmitter location estimator except otherwise stated. In Figure 6, the optimum receiver trajectory obtained from the optimization is shown in red, and the true and estimated trajectory of the transmitter are plotted in black and blue respectively. In these

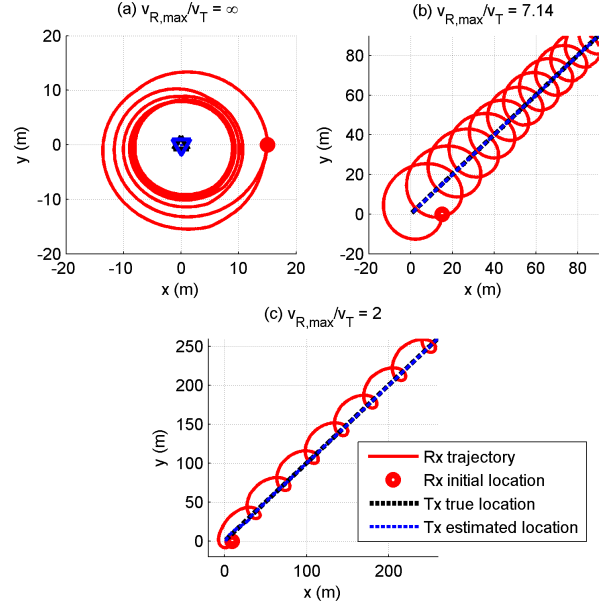


Fig. 6. Receiver trajectory optimization and position estimation of static and moving transmitters. (a) Static transmitter placed at (0,0), (b) a moving transmitter with speed of $v_T = 4.2$ m/s and $v_{R,\max} = 30$ m/s, and (c) a moving transmitter with speed of $v_T = 1.5$ m/s and $v_{R,\max} = 3$ m/s.

figures, the initial position of the receiver is shown with a red circle.

In the first scenario, we consider a fixed transmitter placed at position (0,0). We try to simultaneously locate the transmitter and determine the receiver's optimum trajectory. The maximum receiver speed is $v_{R,\max} = 5$ m/s, and the initial position of the receiver is (15,0). The result of this simulation, demonstrated in Figure 6 (a), shows that the optimum trajectory of the receiver converges to a circle around the transmitter with radius equal to d_{\min} . We note that in all the simulations, the receiver always moves at the maximum allowed speed $v_{R,\max}$. In the second scenario, we consider a transmitter moving with constant velocity. The transmitter speed is set to $v_T = 4.2$ m/s and the receiver maximum speed is $v_{R,\max} = 30$ m/s. The optimum trajectory is shown in Figure 6 (b). The receiver moves in a spiral around the estimated position of the transmitter. In the third scenario, we decrease the receiver-to-transmitter speed ratio $v_{R,\max}/v_T$. We see in Figure 6 (c) that, when $v_{R,\max}/v_T$ becomes small, the optimum trajectory is an "elongated" version of the spiral shape. The lower the ratio $v_{R,\max}/v_T$, the more elongated the spiral trajectory becomes.

We also evaluate the effect of $v_{R,\max}/v_T$ on the transmitter location estimation error. In these simulations, the transmitter is moving with a speed of $v_T = 10$ m/s, and the maximum speed of the receiver is defined so that $\lambda = v_{R,\max}/v_T$ varies from 0.8 to 8. The RMSE of the transmitter location estimation is obtained by averaging over 100 Monte Carlo runs, and shown in Figure 7. In order to provide a common reference point for different values of λ , we assume that the receiver knows the initial position of the transmitter. It can be seen that for $\lambda > 1$, the RMSE first increases and then decreases. This is due to the fact that the initial location of the

transmitter is known, but the transmitter velocity and LO offset are unknown. The transmitter location estimate obtained by the EKF in the early iterations will thus move away from the true transmitter locations, until the EKF is able to provide a better estimate for the transmitter velocity and LO offsets. Eventually, the EKF estimate converges towards the true transmitter location. It is observed that for higher values of λ , the RMSE converges to its steady-state value much faster. The higher the speed of the receiver with respect to that of the transmitter, the lower the maximum and steady-state RMSE becomes. The results also shows that the receiver should move with a speed higher than that of the transmitter for the adaptive filter to converge. This can be understood intuitively as follows: for higher speeds, successive receiver points will be spread further apart, thereby providing more information about the state to be estimated (and most importantly about the transmitter location). At lower speeds, successive receiver points will be located close together, providing little information about the transmitter location.

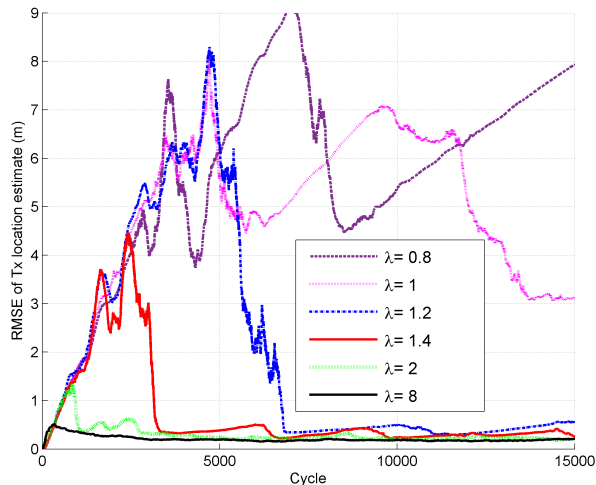


Fig. 7. Root Mean Square Error (RMSE) of location estimation of a moving transmitter for different $\lambda = v_{R,\max}/v_T$.

V. IMPLEMENTATION AND EXPERIMENTAL RESULTS

A. Experimental setup

We evaluate the feasibility of our transmitter localization technique by implementing it on a software-defined radio (SDR) testbed. Both the transmitter and the receiver used in our testbed are USRP-N210, a popular SDR model, equipped with WBX daughterboards [38]. Each SDR is connected to a host processor, which performs the signal processing in real-time with GNU Radio software [39]. The transmitter sends a random pre-generated QPSK message with a 1 MHz bandwidth, at a carrier frequency of 855 MHz. The transmitted message is 1 ms long, and is repeated at a rate of 10 Hz. The receiver's block-diagram is shown in Figure 8. The SDR sends the baseband sample to the host processor with a sample rate of 10 MHz. The baseband samples are processed in real-time: after a low-pass filter, the received

samples are correlated with the known transmitted messages to obtain the TOA of the received packets. Since correlating every incoming sample in real-time is too heavy a burden for a general-purpose processor, a power detector was included between the low-pass filter and the correlator to detect the presence of incoming packets. To increase the resolution beyond 10 MHz, the receiver applies a quadratic interpolation between the three highest points of the correlation function [28], [40]. Lab results with fixed-length cables show that, at high SNR and in multipath-free situations, the TOA accuracy can be increased to typical values below 5 ns. The receiver is also equipped with a high-precision differential GPS (DGPS) which measures the receiver's position with high accuracy. The receiver's position is measured at a rate of 10 Hz, and converted to x-y coordinates. The TOA and x-y coordinates are then used by the EKF/UKF, which estimates the LO drift and transmitter location. Note that the EKF is implemented in GNU Radio and allows for real-time location, whereas the UKF was implemented and tested off-line with recorded TOA and GPS data. The USRP testbed is mounted on trolleys

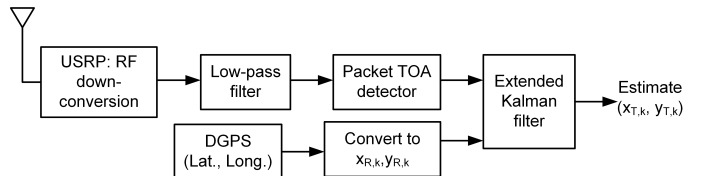


Fig. 8. Block diagram of the receiver. Note that the EKF can be replaced with the UKF without any other change.

which are manually pushed around to move the transmitter and receiver. The measurements were performed in an open environment (e.g. a sports field) to avoid the presence of rich multipath. The speed of the receiver was typically 1.5 m/s, while the speed of the transmitter was low (~ 0.25 m/s). In the case of the moving transmitter, the receiver was moved in a pattern similar to the optimal pattern determined in Section IV.

B. Localization of a static transmitter

The first set of experiments was with a static transmitter. It was determined that, for a static transmitter, the EKF is able to localize the transmitter accurately. The transmitter was placed in the center of the measurement area, and the receiver was moved in a roughly circular trajectory around the transmitter (the distance between transmitter and receiver was roughly 10 m). The initial position of the transmitter in the EKF was set to various random values. The results are shown in Figure 9, for different initial guesses of the transmitter location. Figure 9 illustrates the trajectory of the receiver (in red), the real position of the target (in black) and estimated position of the target (in blue) for different values of (x_0, y_0) in the EKF algorithm. It is observed in Figure 9 that in all cases the algorithm is able to converge toward the true transmitter position.

C. Tracking of a moving transmitter

In a second set of experiments, the transmitter is moved along a straight line. The receiver is moved in a trajectory

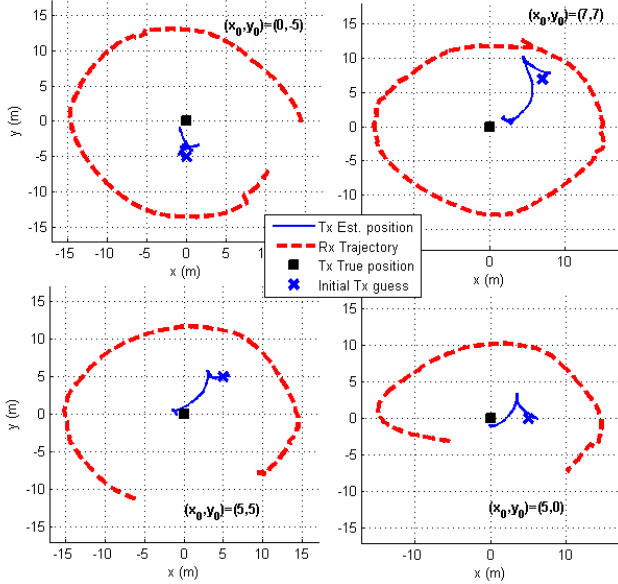


Fig. 9. Position estimation of a static transmitter placed at $(0, 0)$ with different initial guess $(x_0, y_0) = (0, -5), (7, 7), (5, 5)$ and $(5, 0)$.

similar to the optimal trajectories obtained in Section IV. The initial location and direction of the transmitter is assumed to be known. The distance between the transmitter and receiver was kept higher than 5 m at all times. The EKF could only produce appropriate tracking performances when hand-tuning the filter parameters for each measurement, but the UKF was able to provide satisfying result without having to tune the filter parameters for each measurement. Figure 10 shows the tracking capabilities of the UKF for different ratios of receiver-to-transmitter speed v_R/v_T , where v_R and v_T are the receiver and transmitter speeds, respectively. Note that the performance usually degrades towards the end of the measurement run, which is due to the fact that the transmitter and/or the receiver comes to a halt. It can be seen that the best performances are obtained when v_R/v_T is highest. In that case, the receiver is able to perform a wide rotation around the transmitter, providing good resolution along all directions and good tracking performances.

VI. CONCLUSION

We proposed a method to determine the location of a periodic RF transmitter with a mobile receiver. An adaptive filter is used to determine the transmitter location and the LO offset, with the received TOAs and the receiver's locations as inputs. Simulation results showed that the proposed method is able to determine and track the location of the RF transmitter. A simple rule-of-thumb is proposed to determine the localization accuracy of our method, and we show how it is related to the solution of the DARE of the LO-only (linear) adaptive filter. We then investigated which trajectory the receiver should take to optimize the transmitter localization performances by obtaining the PCRLB for this problem and minimizing the trace of it subject to some nonlinear constraints. We showed that for this measurement method, the optimal trajectory of the receiver for a static transmitter is a circular trajectory around

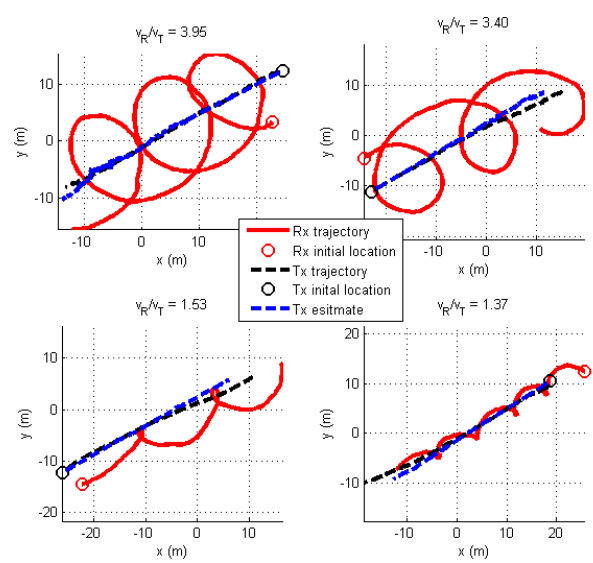


Fig. 10. Tracking performance for a moving transmitter, for different ratios of receiver-to-transmitter speed.

the transmitter. When decreasing the receiver-to-transmitter speed ratio, the optimal trajectory becomes “elongated”. The proposed localization method was successfully implemented on a SDR testbed. Experimental results showed that the localization of a static transmitter could be achieved with a nonlinear filter as simple as an EKF. Tracking of a moving receiver proved to be more difficult, and could only be achieved by using a UKF.

The proposed localization method will be extended to achieve self-localization of vehicles (with a geographically known periodic transmitter) in GNSS-challenged environments. In such situations, the adaptive filtering framework can be augmented to also take into account inertial measurement unit (IMU) measurements. Another exciting prospect is the utilization of virtual AOA measurements for transmitter direction estimation. By estimating the phase of the received periodic messages, the receiver can estimate the AOA of the signal. The challenge lies in separating the AOA phase offset from the phase offset due to LO drift, similar to the V-TDOA case.

REFERENCES

- [1] Y. Bar-Shalom, X. Li, and T. Kirubarajan, *Estimation, Tracking and Navigation: Theory, Algorithms and Software*. New York: John Wiley & Sons, Jun. 2001.
- [2] H. Godrich, A. Haimovich, and R. Blum, “Target localization accuracy gain in mimo radar-based systems,” *IEEE Trans. Inf. Theory*, vol. 56, no. 6, pp. 2783–2803, June 2010.
- [3] W. P. Tay, “The value of feedback in decentralized detection,” *IEEE Trans. Inf. Theory*, vol. 58, no. 12, pp. 7226–7239, Dec. 2012.
- [4] J. Unnikrishnan and V. V. Veeravalli, “Cooperative sensing for primary detection in cognitive radio,” *IEEE J. Sel. Topics Signal Process.*, vol. 2, no. 1, pp. 18–27, 2008.
- [5] Y. Zhang, W. P. Tay, K. H. Li, and D. Gaiti, “Distributed boundary estimation for spectrum sensing in cognitive radio networks,” *IEEE J. Sel. Areas Commun.*, vol. 32, no. 11, pp. 1961–1973, Nov. 2014.
- [6] J. Zheng and Y.-C. Wu, “Joint time synchronization and localization of an unknown node in wireless sensor networks,” *IEEE Trans. Signal Process.*, vol. 58, no. 3, pp. 1309–1320, March 2010.

- [7] J. Caffery and G. Stuber, "Overview of radiolocation in CDMA cellular systems," *IEEE Commun. Mag.*, vol. 36, no. 4, pp. 38–45, Apr 1998.
- [8] F. Gustafsson and F. Gunnarsson, "Mobile positioning using wireless networks: possibilities and fundamental limitations based on available wireless network measurements," *IEEE Signal Process. Mag.*, vol. 22, no. 4, pp. 41–53, July 2005.
- [9] Y. Qi, H. Kobayashi, and H. Suda, "Analysis of wireless geolocation in a non-line-of-sight environment," *IEEE Trans. Wireless Commun.*, vol. 5, no. 3, pp. 672–681, March 2006.
- [10] J. Twigg, J. Fink, P. Yu, and B. Sadler, "RSS gradient-assisted frontier exploration and radio source localization," in *Proc. IEEE Int. Conf. on Robotics and Automation (ICRA)*, May 2012, pp. 889–895.
- [11] C. Feng, W. Au, S. Valaee, and Z. Tan, "Received-signal-strength-based indoor positioning using compressive sensing," *IEEE Trans. Mobile Comput.*, vol. 11, no. 12, pp. 1983–1993, Dec 2012.
- [12] M. Leng, W. P. Tay, T. Q. S. Quek, and H. Shin, "Distributed local linear parameter estimation using Gaussian SPAWN," *IEEE Trans. Signal Process.*, vol. 63, no. 1, pp. 244–257, Jan. 2015.
- [13] Y. Shen and M. Win, "Fundamental limits of wideband localization – part i: A general framework," *IEEE Trans. Inf. Theory*, vol. 56, no. 10, pp. 4956–4980, Oct 2010.
- [14] T. Sathyan, A. Sinha, and T. Kirubarajan, "Passive geolocation and tracking of an unknown number of emitters," *IEEE Trans. Aerosp. Electron. Syst.*, vol. 42, no. 2, pp. 740–750, April 2006.
- [15] H. Jamali-Rad and G. Leus, "Sparsity-aware TDOA localization of multiple sources," in *Proc. IEEE Int. Conf. on Acoust., Speech and Signal Process. (ICASSP)*, May 2013, pp. 4021–4025.
- [16] W. Xu, F. Quitin, M. Leng, W. P. Tay, and S. G. Razul, "Distributed localization of a RF target in NLOS environments," *IEEE J. Sel. Areas Commun.*, 2015.
- [17] M. Leng and W. P. Tay, "Fundamental limits of self-localization for cooperative robotic platforms using signals of opportunity," in *Cooperative Robots and Sensor Networks*. New York, NY: Springer, 2015.
- [18] Y. Wang and K. Ho, "TDOA Source Localization in the Presence of Synchronization Clock Bias and Sensor Position Errors," *IEEE Trans. Signal Process.*, vol. 61, no. 18, pp. 4532–4544, Sept 2013.
- [19] M. Leng, W. P. Tay, C. See, S. Razul, and M. Win, "Modified CRLB for cooperative geolocation of two devices using signals of opportunity," *IEEE Trans. Wireless Commun.*, vol. 13, no. 7, pp. 3636–3649, July 2014.
- [20] M. Malmirchegini, A. Ghaffarkhah, and Y. Mostofi, "Impact of motion and channel parameters on the estimation of transmitter position in robotic networks," in *Proc. IEEE Globecom. Workshops (GC Wkshps)*, Dec 2012, pp. 1538–1543.
- [21] S. Venkateswaran, J. Isaacs, K. Fregene, R. Ratmansky, B. Sadler, J. Hespanha, and U. Madhow, "RF source-seeking by a micro aerial vehicle using rotation-based angle of arrival estimates," in *Proc. American Control Conf. (ACC)*, 2013, June 2013, pp. 2581–2587.
- [22] J. Isaacs, C. Magee, A. Subbaraman, F. Quitin, K. Fregene, A. Teel, U. Madhow, and J. Hespanha, "GPS-optimal micro air vehicle navigation in degraded environments," in *Proc. American Control Conf. (ACC)*, June 2014, pp. 1864–1871.
- [23] J. Isaacs, F. Quitin, L. Garcia Carrillo, U. Madhow, and J. Hespanha, "Quadrotor control for RF source localization and tracking," in *Int. Conf. on Unmanned Aircraft Syst. (ICUAS)*, May 2014, pp. 244–252.
- [24] A. N. Bishop, B. Fidan, B. D. O. Anderson, K. Dogancay, and P. N. Pathirana, "Optimality analysis of sensor-target localization geometries," *Automatica*, vol. 46, no. 3, pp. 479 – 492, 2010.
- [25] R. Kaune and A. Charlish, "Online optimization of sensor trajectories for localization using TDOA measurements," in *Proc. Int. Conf. on Informat. Fusion (FUSION)*, July 2013, pp. 484–491.
- [26] E. F. Sameera S. Ponda, Richard M. Kolacinski, "Trajectory optimization for target localization using small unmanned aerial vehicles," in *Proc. AIAA Guidance, Navig., and Control*, 2009.
- [27] E. Tzoreff, B. Bobrovsky, and A. Weiss, "Single receiver emitter geolocation based on signal periodicity with oscillator instability," *IEEE Trans. Signal Process.*, vol. 62, no. 6, pp. 1377–1385, March 2014.
- [28] F. Quitin, Z. Madadi, and W. P. Tay, "RF transmitter geolocation based on signal periodicity: concept and implementation," in *Proc. IEEE Int. Conf. on Commun. (ICC)*, 2015.
- [29] Z. Madadi, F. Quitin, and W. P. Tay, "Periodic RF transmitter Geolocation using a mobile receiver," in *Proc. IEEE Int. Conf. on Acoust., Speech and Signal Process. (ICASSP)*, 2015.
- [30] C. Zucca and P. Tavella, "The clock model and its relationship with the allan and related variances," *IEEE Trans. Ultrason., Ferroelectr., Freq. Control*, vol. 52, no. 2, pp. 289–296, Feb 2005.
- [31] D. Brown, P. Bidigare, and U. Madhow, "Receiver-coordinated distributed transmit beamforming with kinematic tracking," in *Proc. IEEE Int. Conf. on Acoust., Speech and Signal Process. (ICASSP)*, March 2012, pp. 5209–5212.
- [32] F. Quitin, M. M. U. Rahman, R. Mudumbai, and U. Madhow, "A scalable architecture for distributed transmit beamforming with commodity radios: Design and proof of concept," *IEEE Trans. Wireless Commun.*, vol. 12, no. 3, pp. 1418–1428, March 2013.
- [33] S. Challa, M. Morelande, D. Musicki, and R. Evans, *Fundamentals of Object Tracking*. Cambridge University Press, 2011.
- [34] Y. Bar-Shalom, T. Kirubarajan, and X.-R. Li, *Estimation with Applications to Tracking and Navigation*. New York, NY, USA: John Wiley & Sons, Inc., 2002.
- [35] P. Tichavsky, C. Muravchik, and A. Nehorai, "Posterior Cramer-Rao bounds for discrete-time nonlinear filtering," *IEEE Trans. Signal Process.*, vol. 46, no. 5, pp. 1386–1396, May 1998.
- [36] L. Zuo, R. Niu, and P. Varshney, "Conditional posterior cramer-rao lower bounds for nonlinear sequential bayesian estimation," *IEEE Trans. Signal Process.*, vol. 59, no. 1, pp. 1–14, Jan 2011.
- [37] Y. Zheng, O. Ozdemir, R. Niu, and P. Varshney, "New conditional posterior cramer-rao lower bounds for nonlinear sequential bayesian estimation," *IEEE Trans. Signal Process.*, vol. 60, no. 10, pp. 5549–5556, Oct 2012.
- [38] USRP products, <http://www.ettus.com>, 2015.
- [39] GNU radio, <http://gnuradio.org/redmine/projects/gnuradio>, 2015.
- [40] N. El Gemayel, S. Koslowski, F. Jondral, and J. Tschan, "A low cost TDOA localization system: Setup, challenges and results," in *Proc. Positioning Navig. and Commun. (WPNC), 10th Workshop on*, March 2013, pp. 1–4.